CDF/PHYS/ELECTROWEAK/PUBLIC/10908
Draft 1.5
December 18, 2012

$Z\gamma$ Production in heavy-flavor decay channel at CDF

Timothy Harrington-Taber, Ray Culbertson, Jane Nachtman, Tingjun Yang, Kai Yi

Abstract

We report on the measurement of the cross-section of $p\bar{p} \rightarrow \gamma + Z$ with $Z \rightarrow b\bar{b}$ at CDF, using the entire 9.1 fb^{-1} collected in Run II. We measured $\sigma = 0.36 \pm 0.16(\text{stat.}) \pm 0.11(\text{sys.})$ for events with $E_T^{\gamma} > 15$ GeV, $E_T^{iso} < 1$ GeV, leading jet $E_T > 30$ GeV, secondary jet $E_T > 20$ GeV, jet $|\eta| < 1.5$, $|\eta^{\gamma}| < 1.0$, 50 GeV $< m_{jj} <$ 110 GeV, $m_{\gamma jj} > 80$ GeV, $\Delta R_{j\gamma} > 0.7$, and $\Delta R_{jj} > 1.5$. This is consistent with the value predicted by Pythia of $\sigma = 0.35$ pb.

Contents

1 Introduction

Identification of gauge boson hadronic decays (including heavy flavor) is challenging, as a small two-jet resonance must be extracted from a much larger QCD background. However, being able to identify hadronic resonances present in data dominated by a large QCD background is of critical importance in the search for new particles with dominantly hadronic decays. One such example is the observation of the Higgs boson, for which direct evidence long eluded experimenters.

One major channel for the Higgs search is associated production with an additional vector boson, where the Higgs decays into $b\bar{b}$. However, at the center-of-mass energy $\sqrt{s} = 1.96$ TeV, the standard model (SM) Higgs boson cross section is much smaller than that for similar non-resonant processes, and therefore, sophisticated techniques are required to suppress the QCD background while preserving a high signal detection efficiency.

Considering this, identifying dijet resonances of Z bosons provides an interesting test bench for developing such techniques, due to increased statistical sample and the fact that their characteristics are known from independent analyses. Also, if a Z boson dijet mass peak can be developed with sufficient statistics, it could be a useful tool to constrain the jet energy scale and improve dijet mass resolution, two important factors in any precision measurement of signatures with final state jets.

We are able to improve upon a previous search for hadronic decays of W and Z bosons at CDF [10] by using the complete Run II dataset and requiring b-flavor jets. This is the first analysis for that specifies heavy flavor for the products of the Z decay.

Since the $\gamma+Z$ cross section is larger than heavier diboson cross sections, it provides in principle an excellent opportunity to identify the $Z \to b\bar{b}$ resonance.

As well as providing insight into future gauge boson searches in heavy flavor channels, diboson production with a photon is of independent interest, since $\gamma + Z$ production is correlated to the non-Abelian character of electroweak theory, and is sensitive to certain physics beyond the standard model through possible contributions of $ZZ\gamma$ and $Z\gamma\gamma$ couplings forbidden in the standard model. Such effects have been searched for in leptonic channels, but testing for the presence of similar events in heavy flavor channels could allow for a more stringent test of the SM in this sector.

2 Analysis Overview

In this paper we report on a search for a Z decaying to two heavy-flavor jets based on a sample of $\gamma+b\bar{b}$ data collected throughout CDF Run II, corresponding to an integrated luminosity of 9136 ± 548 pb^{-1}. A previous study, using inclusive hadronic channels rather than specific heavy flavor analysis, performed by the CDF collaboration using 184 pb^{-1} of data was able to set a limit on $\gamma+W(Z)$ production. [10] Specifying heavy-flavor jets together with the improved data sample allows for improved sensitivity in the present analysis.

For this analysis, we distinguish between $p\bar{p} \rightarrow Z\gamma \rightarrow \gamma b\bar{b}$, which we designate ISR (Initial State Radiation), and $p\bar{p} \rightarrow Z \rightarrow \gamma b\bar{b}$, which we designate FSR (Final State Radiation). We used MadGraph [14] to simulate the parton-level interactions and Pythia [13] to simulate the showering and detector-level effects. We prepared Monte Carlo samples to simulate both ISR and FSR events, as well as an additional Monte Carlo sample model our primary irreducible background, which is standard QCD production of $\gamma b\bar{b}$ (explicitly forbidding Z production). The signal Monte Carlo was generated using MadGraph 4 (equivalent to 1682 fb^{-1} for ISR and 3045 fb^{-1} for FSR), and the background Monte Carlo (equivalent to 45.3 fb^{-1})was generated using MadGraph 5, version 1.3.30, where we explicitly specify there is up to 1 additional parton in the MadGraph events and we use MLM matching to eliminate the possibility of double-counting of partons from Pythia showering. Since ISR is more kinematically distinct from this primary background, this analysis is optimized to preferentially select ISR.

2.1 Trigger Efficiency

The trigger used in this analysis, which selects events with a γ candidate and heavy flavor jets, is not perfectly efficient, so we model its behavior by considering a related data sample. The analysis requires that reconstructed and calibrated $E_T^\gamma > 15$ GeV to avoid threshold effects from the γ portion of the trigger, and the additional requirements are applied to the Monte Carlo so that element of the trigger is replicated, and need not be separately simulated We apply a 1 GeV cut on isolation energy to both data and Monte Carlo to duplicate the trigger cut.

To evaluate the efficiency of our trigger, we consider a generally more inclusive dataset, and select events which contain at least one b-tagged jet (jet $E_T > 15$ GeV, $|\eta^j| < 1.5$). Since no b-tagging algorithm is completely pure, we use profile matching (using the Roofit [9] analysis package for all fitting in this analysis) on the secondary vertex mass to estimate the contribution of light flavor, charm jets, and b jets to the total secondary vertex mass profile for b-tagged jets. To determine the efficiency of the trigger, we compare the estimated number of b flavor jets that pass the SVT trigger (shown in Figure 1(b))to the estimated number present without requiring the SVT trigger, as shown in Figure 1(a), repeating this for different ranges of jet energy. Secondary vertex mass templates were obtained using MC simulation (generated using Pythia). As seen in Figure 2.1 the efficiency, while consistent with being constant, does show a slight increase at higher transverse energy.

Throughout the remainder of the analysis, all Monte Carlo events will be weighted by the trigger efficiency here, based on the E_T of their leading jet.

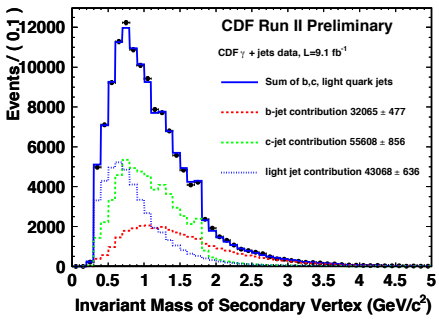

(a) Inclusive.

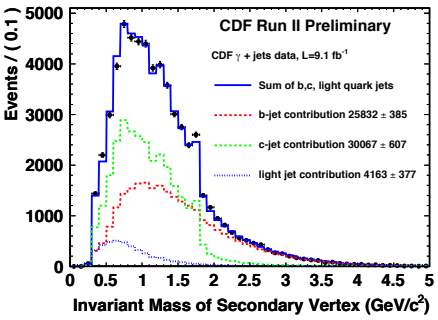

(b) Pass SVT trigger.

Figure 1: Mass associated with secondary vertex for jets passing inclusive γ trigger, using the full jet E_T range of 20-140 GeV.

3 Event Selection

For our analysis, we require that events have 2 b-tagged jets and an isolated photon candidate. We also require that the jets and γ both be central, that is, jet $|\eta| < 1.5$ and $|\eta^\gamma| < 1.0$.

To increase the purity of the photon sample, we require that photon candidates pass a standard photon ID neural network cut of 0.85[2]. We also applied a number of kinematic cuts in order to reduce the presence of background and possible trigger artifacts. As such, we place a 15 GeV transverse energy requirement on photons, require leading jet transverse energy exceed 30 GeV, secondary jet transverse energy exceed 20 GeV, that the reconstructed dijet mass is between 50 and 110 GeV, that the reconstructed mass of the photon and two jets exceeds 110 GeV, as well as some cuts on the spacing and location of the jets. Analysis cuts are summarized in table 1. This gives us 1555 data events which pass this set of cuts, to be used in our analysis. These cuts were chosen so as to limit the amount of background present without signficantly reducing the ISR content of the data.

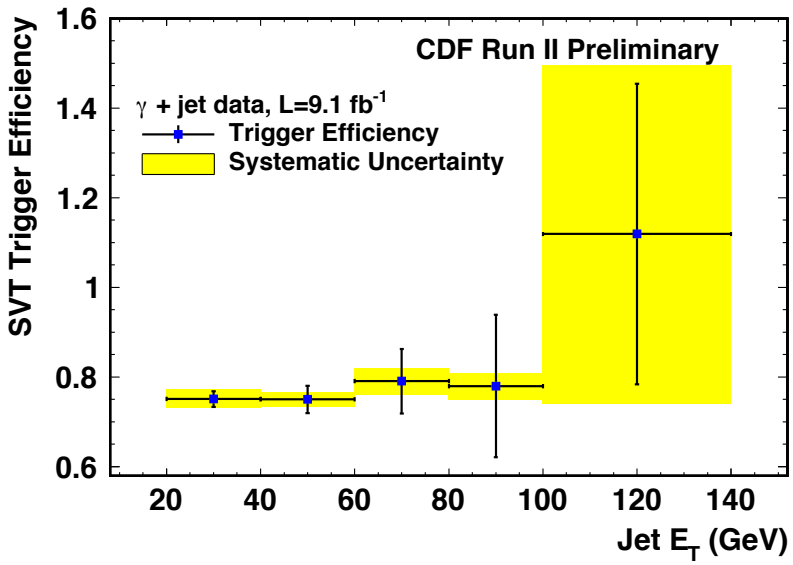

Figure 2: SVT trigger efficiency as a function of jet E_T.

4 Background Estimation and Signal Yield

The principle challenge in this analysis is to distinguish between the various sources of background events and $\gamma + Z$ events. The selection process requires a signature of $\gamma b\bar{b}$ present in the reconstruction of the event, so background can be described as a combination of those events whereby one or more elements is mistakenly reconstructed so as to imitate the selected signature and those events whereby the requisite signature is produced through other channels besides that of the desired $\gamma + Z$ production.

Events which imitate the desired signature may be broadly classed into two cate-

Table 1: Summary of cuts implemented in this analysis, excluding trigger requirements.

E_T^γ	> 15 GeV
Leading jet E_T	> 30 GeV
Secondary jet E_T	> 20 GeV
m_{jj}	$50 < m_{jj} < 110$ GeV
$m_{\gamma jj}$	> 80 GeV
$\Delta R(\gamma, j_1)$	> 0.7
$\Delta R(\gamma, j_2)$	> 0.7
$\Delta R(j_1, j_2)$	> 1.5
Jet $\lvert\eta\rvert$	< 1.5
$\lvert\eta^\gamma\rvert$	< 1.0

gories: those events where the γ reconstructed by the event is the product of a mesonic decay (such as a π^0 decay), rather than the prompt production characteristic of the signal; and those events where one or more b-tagged jets do not actually contain a b quark. Due to the relevant production cross-sections, production of $\gamma b\bar{b}$ is dominated by QCD processes. Background due to inaccurate reconstruction will be modeled using data sidebands to represent the processes as accurately as possible, whereas QCD $\gamma b\bar{b}$ production is modeled using Monte Carlo simulated data.

In order to ascertain the prevalence of events with mistaken reconstruction, the data distribution for a relevant parameter is fitted to a mixture of MC templates, one of which contains a simulation of background events, but which are sometimes reconstructed as passing the analysis cuts, while another contains the intended signal.

As there still remains significant QCD background which cannot be readily distinguished from the Z related events, a neural network is developed to distinguish between $\gamma b\bar{b}$ events related to QCD production and Z production. The data is then fitted to four templates, one of fixed normalization modeling the presence of those events with a non-prompt γ (that is, γ produced by the decay of another particle, rather than those generated at the primary vertex), one of fixed normalization modeling those events with one or more jets tagged as b-flavor (which pass the γ neural network cut), but actually of lighter flavor, and two whose normalization is determined by the fitting algorithm for the signal and primary QCD $\gamma b\bar{b}$ background.

4.1 Fake photon sideband estimation and modeling

To estimate the presence of fake γ in our data sample, we model the number of non-prompt photons that pass our photon ID neural network cut. To do so, we plot the photon ID neural network output for our data sample (excluding the photon ID cut) and use our QCD Monte Carlo sample to obtain templates for prompt and non-prompt photons. The data profile is then fitted to a combination of these two templates, which

yields an estimate of how many decay product γ are present in the data that will pass the photon ID cut. This plot, with fit values shown for the entire range of γ ann outputs, is shown in Figure 3. We expect that, out of our 1555 data events, $134.7 \pm 9.0(\text{stat.}) \pm 29.8(\text{sys.})$ are due to non-prompt photons being reconstructed as prompt photons.

To model the effect of the template shape of this background on the final neural network fit, we consider those data events that pass all other analysis cuts, but which have a photon neural network ID output between 0.15 and 0.85, as a sideband. We use the normalization calculated above and use this as an element of our fit. Errors associated with uncertainties in the rate are determined by adjusting the normalization of the sideband in accordance with our uncertainty. The combined rate and shape systematic uncertainties for this sideband turn out to be our smallest systematic effect.

4.2 Fake b-jet sideband estimation and modeling

As our estimation of trigger efficiency suggests, not all jets tagged by Tight SecVtx contain a b quark. In order to correct for this, we look at the two-dimensional distribution of secondary mass vertex of the two leading jets (secondary mass vertex for the second jet versus secondary mass vertex of the leading jet) for the data sample. Then, we fit this distribution to a combination of three templates: a fake γ sideband template derived from data which does not pass the photon neural network cut, with normalization fixed by our estimate for that parameter; a Monte Carlo template of those events with two b jets, whose normalization is determined by the fitting algorithm; and a Monte Carlo template of those events with at least one non-b jet, with the normalization also variable as a fit parameter. The projection of this fit along each axis is shown in Figure 4. For the final neural network fit, we model the presence of these fake b events using a data sideband which passes all other analysis cuts, but which has exactly 0 b tagged jets.

4.3 Neural network development and fitting

Figure 5 shows the distribution of m_{jj} with the analysis cuts in place. As the separation between signal and background is insufficient to obtain a satisfactory fit by fitting directly to the dijet (or three-body) mass, more rigorous tools will need to be developed. Therefore, we used the built-in Root libraries to develop a neural network to distinguish between our QCD $\gamma b\bar{b}$ production and our ISR γZ where $Z \to b\bar{b}$. To select our input parameters, we required that these events show clear distinction between these two samples and that the data was reasonably well-modeled by the QCD MC sample. We therefore selected the following 8 variables:

- m_{jj}, reconstructed dijet mass
- $m_{\gamma jj}$, reconstructed three-body mass

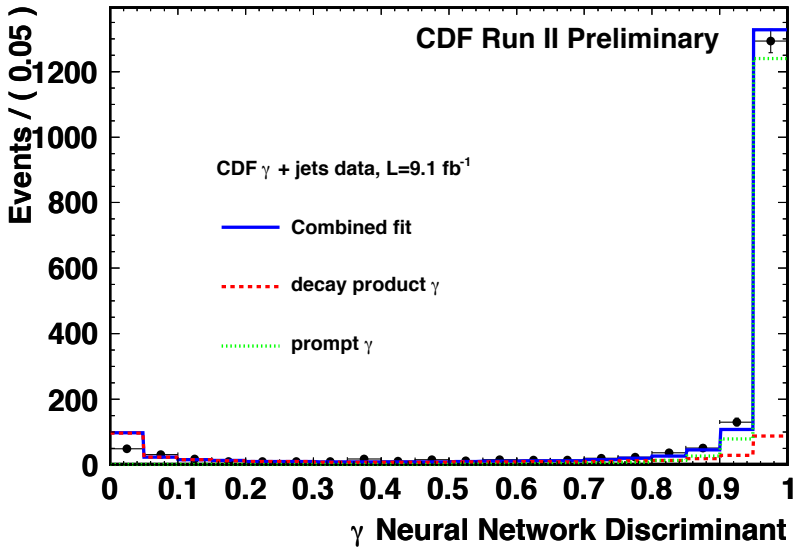

Figure 3: Fitted γ ann neural network output. Used to estimate presence of 135 ± 31 fake γ events in γ + jets data.

- E_T^{j1}, leading jet transverse energy
- E_T^{j2}, secondary jet transverse energy
- $\Delta R(\gamma, j_1)$, separation between leading jet and photon
- $\Delta R(\gamma, j_2)$, separation between secondary jet and photon
- $\Delta\phi_{jj}$, difference in azimuthal angle between jets

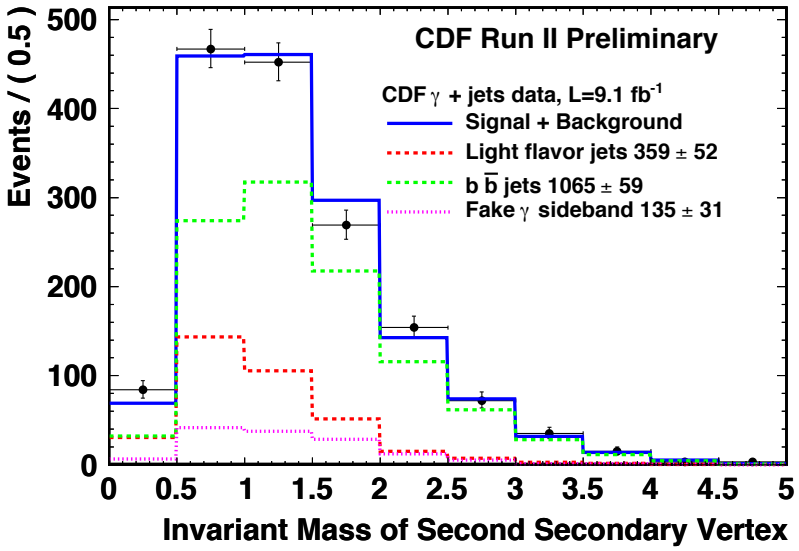

Figure 4: One-dimensional projection of secondary vertex mass distribution fit for leading jet E_T between 20 and 140 GeV.

- $\Delta\eta_{jj}$, difference in pseudorapidity angle between jets

The output of the neural network, as applied to the data sample, is then fitted to obtain the signal yield, as shown in Figure 6. The fake b and fake γ sidebands have their normalization fixed by our estimates as to their presence. The signal population is estimated as being 90% ISR and 10% FSR (based on relative MadGraph cross-section for analysis cuts). The data output is then fitted, with the normalization of the MC signal and MC QCD background templates determined by the RooFit analysis

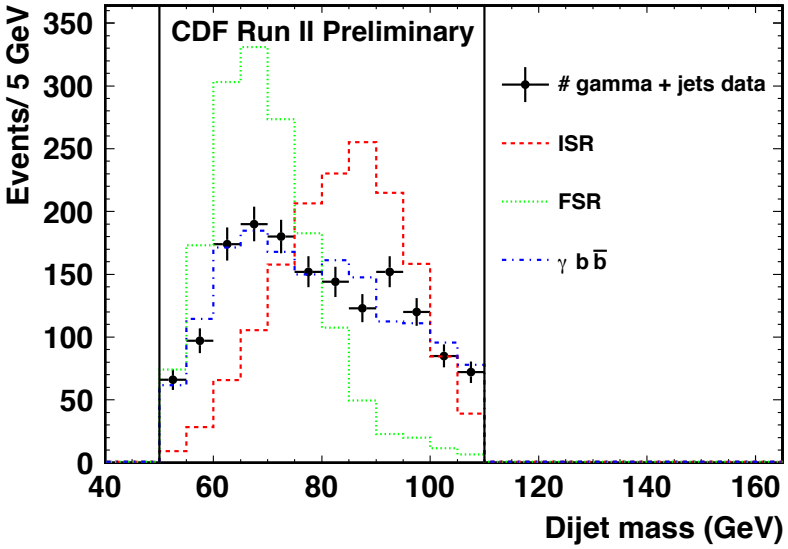

Figure 5: Dijet mass distribution for data and various Monte Carlo samples (Monte Carlo templates normalized to data).

algorithm, with results summarized in Table 2. Note that the statistical uncertainty is still quite large relative to estimated signal yield. This is the dominant uncertainty in this analysis and is likely due at least in part to the relatively large amount of irreducible background relative to the amount of signal. To illustrate the quality of the fit, we reconstruct several kinematic quantities in Figures 7 through 12, with the normalization for each component based on our fit estimate as to its presence in data, as shown in Table 2.

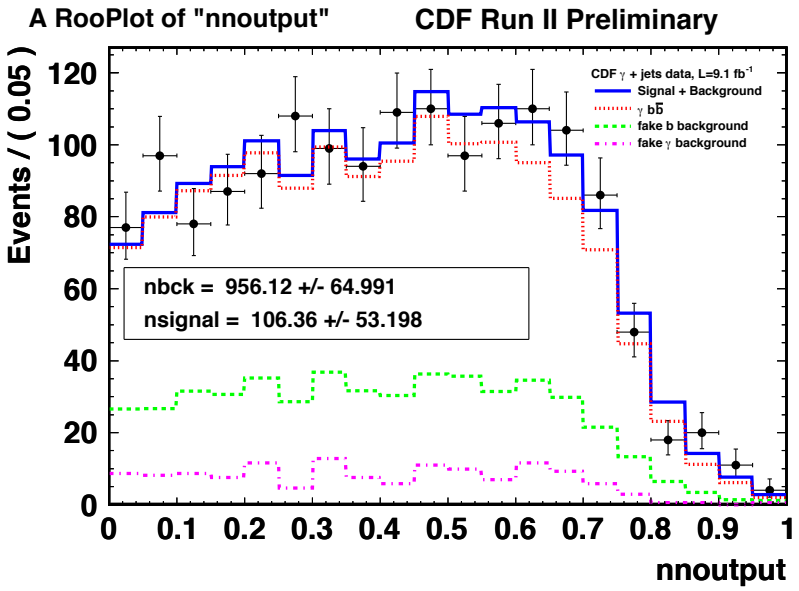

Figure 6: Fit of neural network output, with components shown stacked on the plot.

5 Cross Section Estimation

Cross section was calculated using the relation $\sigma = N/L\epsilon$, where σ is the cross section, N the number of events in the signal yield, L the integrated luminosity, and ϵ the unfolding factor. A careful analysis of our processes shows that several factors will have significant impacts on cross section measurements. For ease of reference, these are included here.

Table 2: Elements of (uncorrected) neural network fit. Sidebands are normalized based on predicted presence, while $\gamma b\bar{b}$ and γZ content is determined by the fitting algorithm.

Fit Component	Number of Events
Fake γ sideband	134.7
Fake b-jet sideband	358.7
Fitted $\gamma b\bar{b}$	956.1
Fitted γZ	106.4

5.1 Unfolding Factor

Since the unfolding factor (ϵ) incorporates all of the trigger and selection efficiencies, it is readily calculated by determining the number of parton level Monte Carlo events that pass the kinematic cuts and comparing that to the number of reconstructed events that satisfy the same cuts, with the distribution as a function of E_T^γ shown in Figure 13. This plot was obtained by dividing two histograms, each derived from our Monte Carlo sample. The numerator was simply those events that passed our analysis cuts, as weighted for SVT trigger efficiency. The denominator was those Monte Carlo events where the generator level information satisfied the kinematic cuts ($\gamma E_T > 15$ GeV, $E_T^{iso} < 1$ GeV, $|\eta^\gamma| < 1$, jet $|\eta| < 1.5$, leading jet $E_T > 30$ GeV, secondary jet $E_T > 20$ GeV, 50 GeV $< m_{jj} <$ 110 GeV, $m_{\gamma jj} > 80$ GeV, $\Delta R_{j\gamma} > 0.7$, and $\Delta R_{jj} > 1.5$). However, this neglects cases where the Monte Carlo efficiency does not match the data efficiency. The uncertainties associated with these reconstructions are detailed in Table 3. We calculate our unfolding factor to be $\epsilon = .0362 \pm .0003(\text{stat.}) \pm .0049$ (sys.). However, since some sources of uncertainty in unfolding factor are directly correlated with changes in yield, we break down uncertainties in unfolding factor and independently determine their impact upon the final cross section.

Table 3: Percentage changes in uncertainty of unfolding factor due to various systematic effects

Source of uncertainty	Impact upon unfolding factor
SVT trigger rate	8.3%
Jet energy scale	5.1%
γ energy scale	2.0%
γ acceptance	2.0%
b acceptance	7.1%
Total systematic uncertainty	13.5%

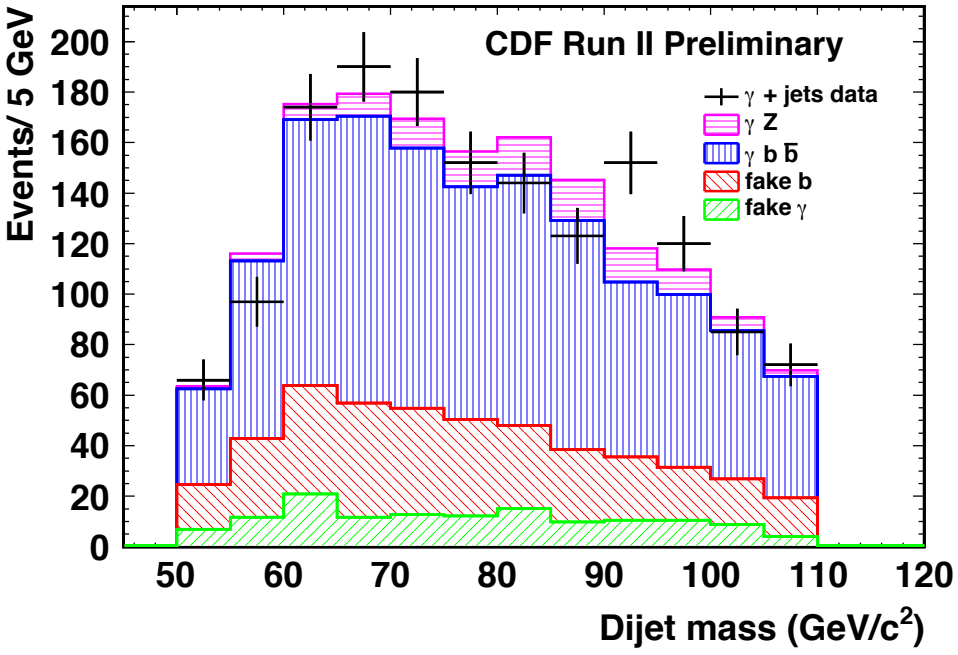

Figure 7: Reconstructed m_{jj} for composite fit.

5.2 Systematic Effects from PDF Uncertainties

Since Monte Carlo generation and cross section estimation is highly dependent upon the relative likelihood of a particular parton being the active element in a particular in-

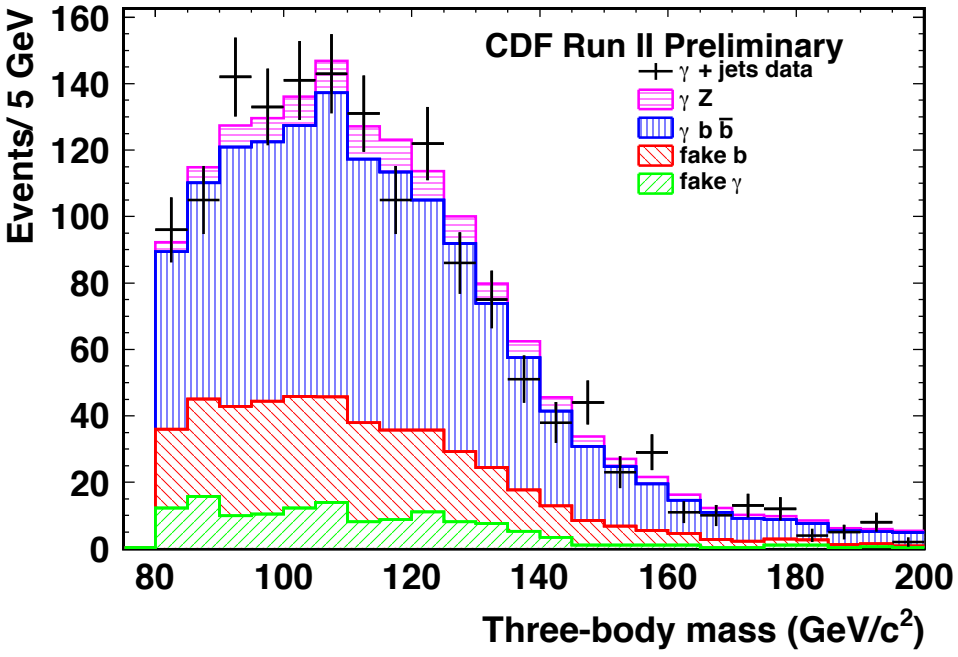

Figure 8: Reconstructed three-body invariant mass for composite fit.

teraction, any uncertainties in these parameters (which cannot, of course, be measured directly) will impact any dependent result. As we used the 20 orthogonal CTEQ6M[12] eigenvectors to reweight our Monte Carlo sample, we also possess the relative weight-

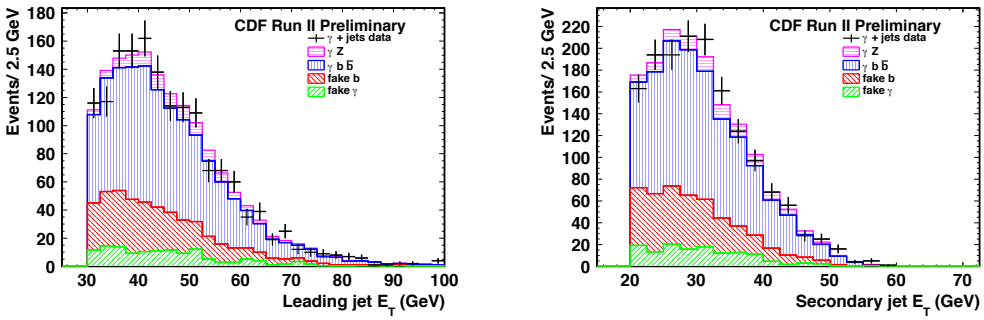

(a) Leading jet E_T (b) Secondary jet E_T

Figure 9: Transverse energy associated with each jet, normalized to match composite fit.

ings for each event according to these eigenvectors. In order to evaluate the associated systematic effect, we can re-weight our Monte Carlo events in accordance with each of these separate eigenvectors (twice, $\pm 1\sigma$, for each eigenvector), and fit the templates for Monte Carlo samples reweighted in this way determine the impact of each particular uncertainty upon our neural network fit. The larger deviation for each eigenvector is taken to be the associated uncertainty, and these 20 values are then added in quadrature to obtain a total uncertainty associated with pdf weighting. This suggests an uncertainty in yield of 16.1 signal events (effect on cross section detailed in Table 7).

5.3 Systematic Effects from Photon Energy Scale

As γ energy determines acceptance for events, we need to evaluate the impact of the uncertainty in energy scale upon our analysis. As this scale is relatively well-defined, we observe the effects of a 1.5 percent shift in photon transverse energy on our fit [3] (when we shift the energy scale on the Monte Carlo templates) and on the unfolding factor (where it is applied to the reconstructed events). These results partially cancel each other out, and correlate to an uncertainty of roughly one percent in the cross section. As this effect is relatively minimal, a more detailed analysis of this effect is not deemed necessary.

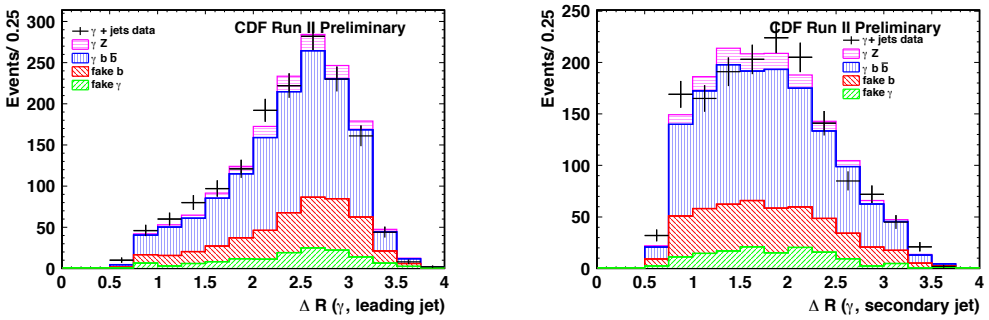

(a) $\Delta R(\gamma, leading jet)$ (b) $\Delta R(\gamma, secondary jet)$

Figure 10: Angular separation between γ and jets, normalized to match composite fit.

5.4 Systematic Effects from Jet Energy Scale

As jet energy scale is a larger uncertainty at CDF, its impacts merit a more careful study. In addition, since we use no less than four neural network variables dependent upon our jet energy scale (as reconstructed mass is dependent upon measured transverse energy of the jets), we expect this analysis to be especially sensitive to this effect. Thus, we compare two different methods of evaluating the associated change in signal yield, taking the larger to be our associated uncertainty. The first method is simply to repeat the fit with the input parameters shifted for the MC events in accordance with the scale uncertainties. The second is to fit the shifted Monte Carlo templates to the unbiased fit result profile for the same templates (that is, to change the shape of the templates according to the shift in jet energy scale, and then fit the new templates to the old shape, to reduce the impact of the statistical fluctuations in the data). This method is intended to reduce the impact of the statistical fluctuations in the data. As the latter method suggests a larger uncertainty (a change of 30 in signal yield), it is used for this analysis. In a similar manner to the γ energy scale, the jet energy scale systematic uncertainty is slightly reduced by the correlated change in unfolding factor (which, as for the γ energy scale, we calculate by applying the scale shift to the reconstructed events). It still remains the dominant systematic uncertainty in this analysis.

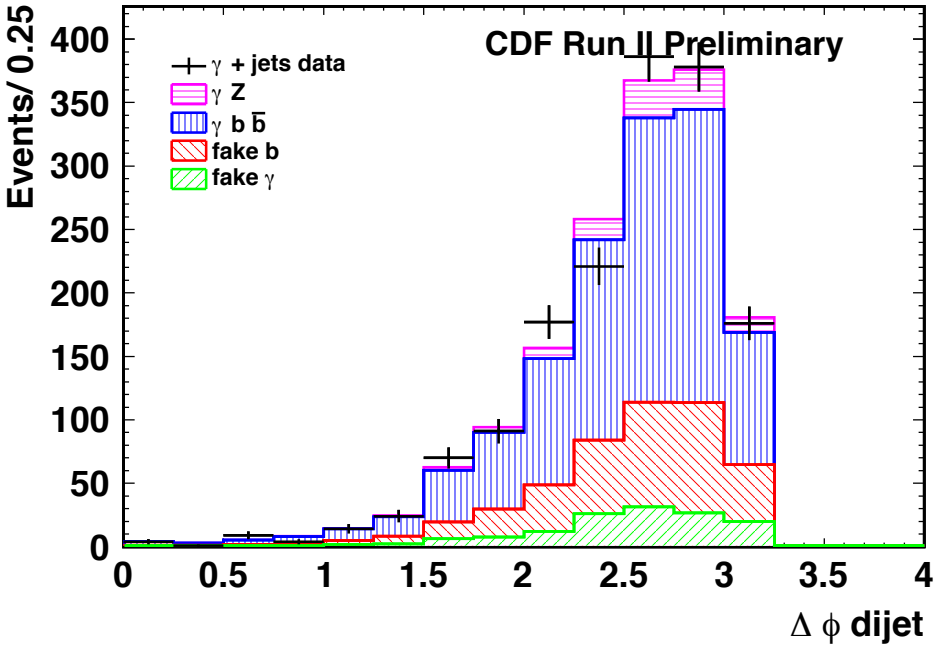

Figure 11: $\Delta\phi$ between the two jets using composite fit normalization.

5.5 Systematic Effects from Fake b Sideband

We also need to consider the uncertainties resulting from the mistag rate of the Tight SecVtx b tagger, both in those jets falsely tagged and in those b jets inaccurately not

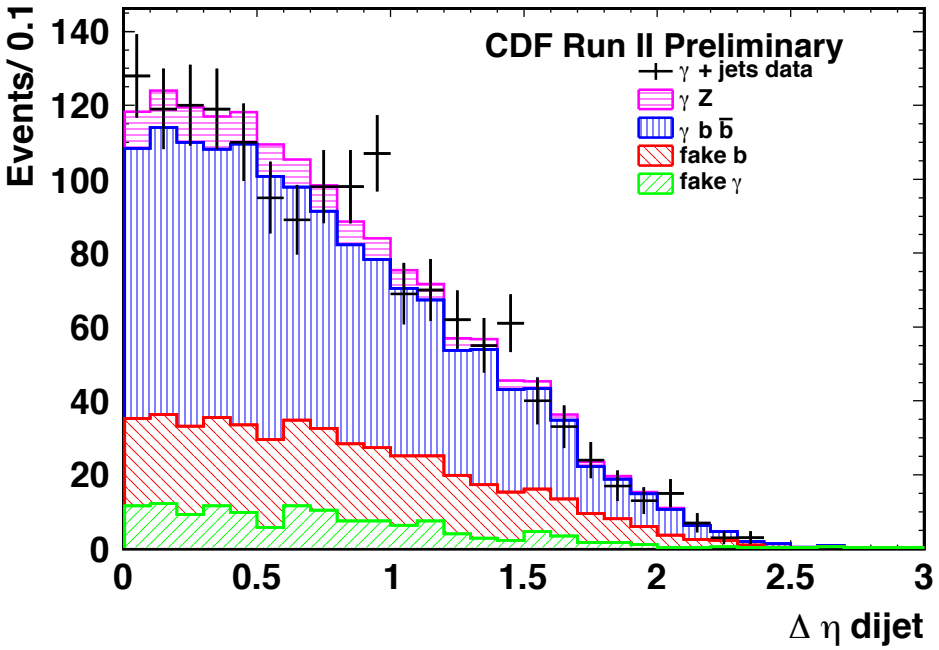

Figure 12: $\Delta\eta$ between the two jets using composite fit normalization.

tagged as such. Table 4 shows that even the data sample with 0 b tags contains some $\gamma b\bar{b}$ events. We model the systematic impact of this presence by constructing additional sideband templates with varying amounts of $\gamma b\bar{b}$ events present. We do this adding

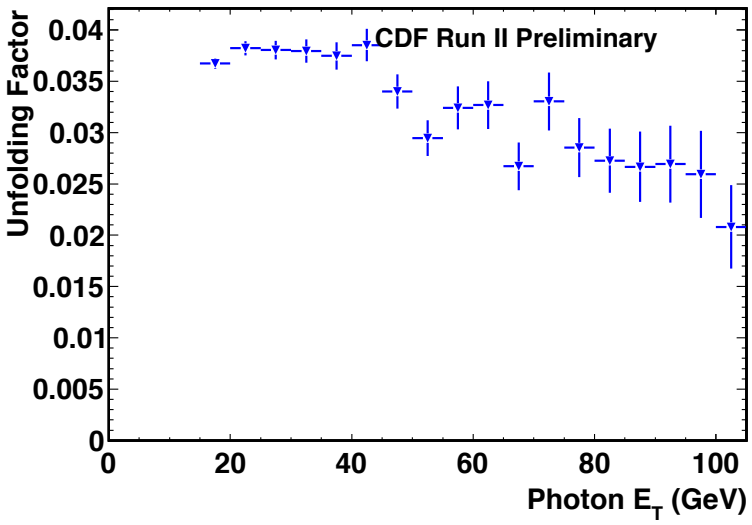

Figure 13: Unfolding factor versus Photon E_t.

the 0-tag sideband to varying amounts of the 1-tag sideband (noting, in passing, that the 0-tag sideband has much larger statistics), and observing the impact of different sidebands on the estimated signal yield. This turns out to be surprisingly consistent, suggesting that the true yield present in the sample is slightly larger than that obtained directly from the fit. Thus, we plot signal yield as a function of $\gamma b\bar{b}$ presence in the fake b sideband, which suggests an actual yield of 120.7 signal events. We take the difference between this and our 0-tag sideband fit (14.3 events) to be a systematic uncertainty in this yield, associated with the fake b sideband. Table 5 shows our best estimate for the composition of the data sample, accounting for this systematic effect.

Table 4: Expected number of events with a given number of b tags for each Monte Carlo predicted data sample, normalization for ISR, FSR, and $\gamma b\bar{b}$based on MadGraph predictions as well as the actual number of events present in the data with that particular number of b tags.

Number of b tags	ISR	FSR	$\gamma b\bar{b}$	data
2+	52.8	5.95	791	1555
1	123	15.8	4196	19074
0	116	19.4	7223	179058

Table 5: Elements of neural network fit, corrected for fake b sideband. Sidebands are normalized based on predicted presence, while $\gamma b\bar{b}$ and γZ content is determined by the fitting algorithm.

Fit Component	Number of Events
Fake γ sideband	134.7
Fake b-jet sideband	358.7
Fitted $\gamma b\bar{b}$	941.8
Fitted γZ	120.7

5.6 Summary of Systematic Effects on Cross Section

Statistical and systematic uncertainties are summarized in Tables 6 and 7. Clearly, the statistical uncertainty associated with the quality of the neural network fit itself is the dominant contribution, with jet energy scale our largest systematic effect. Thus, for our kinematic cuts ($50 < m_{jj} < 110$ GeV, $m_{\gamma jj} > 80$ GeV, leading jet $E_T > 30$ GeV, secondary jet $E_T > 20$ GeV, $E_T^{\gamma} > 15$ GeV, $E_T^{iso} < 1$ GeV, $\Delta R_{j\gamma} > 0.7$, and $\Delta R_{jj} > 1.5$), we have $\sigma = 0.36 \pm 0.16(\text{stat.}) \pm 0.11(\text{sys.})$ pb, consistent with our prediction of $\sigma = 0.35$ pb, obtained by Pythia, using a k-factor of 1.41, which we obtain from the predicted value for hadronic cross sections described in [7] (linear term in fit in source appears to have sign reversed, based on plot shown, which we change).

6 Summary

In this analysis, we are able to measure the cross-section associated with $Z\gamma$ production where $Z \to b\bar{b}$ to be $0.36 \pm 0.16(\text{stat.}) \pm 0.11$ (sys.) pb, consistent with our Monte Carlo prediction of 0.35 pb. This analysis is limited by large statistical uncertainty in the neural network fit, and is also rather sensitive to the jet energy scale. A more sophisticated approach to neural network development might be able to improve the uncertainty achieved.

Table 6: Statistical uncertainties in this analysis and the resulting impact on cross section

Source of Uncertainty	Impact of Uncertainty on Cross Section (pb)
Neural Network Fit	.161
Fake γ Rate	.002
Fake b Rate	.006
Unfolding factor	.004
Total Statistical Uncertainty	.161

Table 7: Systematic uncertainties in this analysis and their impact upon our cross section measurement

Source of Uncertainty	Impact of Uncertainty on Cross Section (pb)
Jet Energy Scale	0.075
Fake b Sideband	0.049
PDF Weighting	0.031
Luminosity	0.022
Fake γ Sideband	0.011
γ Energy Scale	0.003
Unfolding γ efficiency	0.008
Unfolding b efficiency	0.027
SVT trigger rate	0.032
SVT trigger Energy-dependence	0.022
Total Systematic Uncertainty	0.109

References

[1] K. Bland *et al.*, "Search for a SM and fermiophobic Higgs Boson in the Diphoton Final State", CDF Note 10724.

[2] J. Ray *et al.*, "Multivariate Photon ID for CDF", CDF Note 10282.

[3] S. Yu *et al.*, "Studies of Electron and Photon Energy Scales", CDF Note 9591.

[4] V. Giakoumopoulou and J. Freeman, "Summer 2010 SevVtx Scale Factors Calculated Using the Electron Method through Period 28", CDF Note 10178.

[5] S. Sabik and P. Savard, "Track reconstruction efficiency in jets", CDF Note 6894.

[6] R. McNulty and T. Shears, "Photon + b jet production at CDF", CDF Note 8329.

[7] A. Bocci, "Theoretical Prediction of $W\gamma$ and $Z\gamma$ Production in the Hadronic Channel", CDF Note 7664.

[8] http://www-cdf.fnal.gov/internal/physics/top/RunIIBtag/bTag.html.

[9] root.cern.ch/drupal/content/roofit.

[10] T. Aaltonen *et al.* (CDF Collaboration), Phys. Rev. D **80**, 052011 (2009) [arXiv:0803.4264 [hep-ex]].

[11] J. Freeman *et al.*, "Anomalous Coupling Limits from $Z+\gamma$ Production Combining Electronic and Muonic Channels in 5/fb", CDF Note 10043.

[12] J. Pumplin *et al.*, JHEP 0207:012(2002), hep-ph/0201195

[13] T. Sjostrand *et al.*, Comput. Phys. Commun. **135**, 238 (2001).

[14] F. Maltoni and T. Stelzer, JHEP 02 (2003) 027.